European Journal of Medicinal Chemistry 317 (2026) 119122

Contents lists available at ScienceDirect

European Journal of Medicinal Chemistry

journal homepage: www.elsevier.com/locate/ejmech

Research paper

Aromatic π-stacking stabilizes an α-helical SARS-CoV-2 MPER peptide that mimics the post-fusion spike and enables potent antiviral activity

Michael Quagliata [a], Sonja Bazhenova [b], Rosaria Arvia [c], Shima Siadohoni [a], Andrea Di Santo [d], Feliciana Real-Fernandez [e], Anna Maria Papini [a], Simone Giannecchini [c,*], Daniel Friedrich [b,**], Paolo Rovero [d,***]

[a] *Interdepartmental Research Unit of Peptide and Protein Chemistry and Biology, Department of Chemistry "Ugo Schiff", University of Florence, Via Della Lastruccia 13, Sesto Fiorentino, I-50019, Italy*
[b] *Department of Chemistry and Biochemistry, University of Cologne, Greinstraße 4, Cologne, 50939, Germany*
[c] *Department of Experimental and Clinical Medicine, University of Florence, Viale Morgagni 48, Florence, I-50134, Italy*
[d] *Interdepartmental Research Unit of Peptide and Protein Chemistry and Biology, Department of NeuroFarBa, University of Florence, Via Ugo Schiff 6, Sesto Fiorentino, I-50019, Italy*
[e] *CNR - Istituto di Chimica Dei Composti Organometallici (CNR-ICCOM), Via Madonna Del Piano 10, Sesto Fiorentino, I-50019, Italy*

A B S T R A C T

Membrane fusion between SARS-CoV-2 and host cells is mediated by the spike protein and involves the membrane-proximal external region (MPER), a tryptophan-rich sequence implicated in viral entry. Here, we investigated the feasibility of MPER-derived peptides as potential antiviral agents and examined the structural determinants underlying their activity. A series of truncated MPER peptides was synthesized and evaluated for antiviral activity against SARS-CoV-2 in cellular assays, revealing potent inhibitory potency against different variants, with nanomolar IC_{50} values associated with sequences rich in aromatic residues. Notably, this activity was time-dependent, decreasing in effectiveness when the peptide was added 1 h post-infection. Using NMR spectroscopy, we demonstrate that these peptides adopt a stable α-helical conformation in solution and membrane-mimetic environments that is stabilized by intramolecular aromatic π-π stacking interactions among tryptophan and tyrosine side chains. Structure–activity analysis indicates that this aromatic network promotes α-helix stabilization mimicking MPER structure of the spike post-fusion and correlates with enhanced antiviral potency. Our findings reveal a structural mechanism by which aromatic stacking stabilizes MPER helicity and drives antiviral activity, providing insights into peptide-based inhibition of viral membrane fusion and offering a framework for the rational design of SARS-CoV-2 entry inhibitors.

1. Introduction

After the first case of SARS-CoV-2 discovered in Wuhan, China, on 31 December 2019, more than 7 million people died due to complications related to COVID-19 and more than 750 million cases were reported [1]. In August 2021, the FDA approved the first vaccine against the virus [2], a mRNA-based vaccine called Tozinameran (Comirnaty®) developed by Pfizer-BioNTech [3]. At the end of the same year, the FDA also approved the first antiviral specific for treatment of COVID-19, called Molnupiravir (Lagevrio®) and developed by Merck, a modified nucleoside which exerts its antiviral action by introducing copy errors during viral RNA replication [4,5]. These achievements represented significant milestones in the fight against the SARS-CoV-2 pandemic that dramatically affected people worldwide. Despite the discoveries aforementioned, there is a need in developing new and more potent therapeutics as vaccines may become less effective in immunocompromised patients and applications of antivirals decreases the specificity of treatment.

The infection pathway of SARS-CoV-2 involves complex interactions between viral and host cell structures [6]. To exploit the cell machinery for replication, the virus is internalized into the cell in a process called cell-entry. Initially, the *Receptor Binding Domain* (RBD) contained in the subunit S1 of the viral spike protein recognizes the *Angiotensin Converting Enzyme* 2 (ACE2) receptor expressed on the host cell surface [7]. Subsequently, the proteolytic cleavage of the S1 subunit, performed by the host *Transmembrane protease serine 2* (TMPRSS2) or the endosomal cysteine protease cathepsin L, allows the anchoring of *Fusion peptide* (FP) into the cell membrane [8]. This movement triggers the interaction between *Heptad repeat region 1* and *2* (HR2 and HR1) which leads to the

* Corresponding author.
** Corresponding author.
*** Corresponding author.
E-mail addresses: simone.giannecchini@unifi.it (S. Giannecchini), daniel.friedrich@uni-koeln.de (D. Friedrich), paolo.rovero@unifi.it (P. Rovero).

https://doi.org/10.1016/j.ejmech.2026.119122
Received 30 March 2026; Received in revised form 1 July 2026; Accepted 2 July 2026
Available online 8 July 2026

formation of a six-helix bundle (6-HB), bringing the viral membrane closer to the cell membrane and allowing the fusion of the two membranes, leading to virus internalization [9,10]. Notably, all these interactions occur mainly in the extracellular environment, making the cell-entry a promising target to block the infection [11,12].

Fusion inhibitor peptides are a well-known class of compounds capable of interfering with viral cell-entry [13]. The most prominent example is Enfuvirtide (Fuzeon®), an FDA-approved drug used as an HIV fusion inhibitor [14]. However, several viruses share similar mechanisms of membrane fusion to mediate viral cell-entry and therefore this step is particularly attractive for developing antiviral therapeutics [15,16]. In the context of SARS-CoV-2, the intramolecular protein-protein interaction (PPI) involving HR1 and HR2 is well-exploited for developing potential anti-fusion peptides. In fact, several HR2-derived peptides, such as dimers and/or C-terminal cholesterol-modified analogs, have been reported to be effective both *in vitro* and *in vivo* [17–21].

All the peptides reported above exert their activity by interacting with the spike subunit S2 HR1 region, thus blocking the formation of 6-HB, crucial for the subsequent membrane fusion. However, in the case of SARS-CoV, Liao *et* al. discovered that after this 6-HB formation, the subsequent interaction between the *Internal Fusion Peptide* (IFP) and the tryptophan-rich *Membrane Proximity External Region* (MPER), which are located in the *N*- and C-terminal part of the subunit S2, respectively, serves as its molecular extension to facilitate the fusion of viral and host cell membranes [22]. In particular, this study demonstrates the importance of indole rings of tryptophan involved in this binding to fulfill viral-cell membrane fusion. In this context, several studies reported the conservation of MPER tryptophan/aromatic residues in several viruses highlighting their key role in viral cell-entry (*vide supra*). For example, it was demonstrated in a previous study that the membrane-proximal tryptophan-rich ectodomain of the Feline Immunodeficiency Virus (FIV) transmembrane glycoprotein plays a critical role in cell entry [23]. Moreover, the octapeptide C8 (WEDWVRWI) is capable of inhibiting viral replication *in vitro*, with an IC_{50} of 50 nM [24]. Similarly, Regula *et* al. has shown that the MPER domain contained in the GP2 subunit of the Ebola virus (EBOV) envelope glycoprotein mediates viral cell entry [25]. In particular, a conformational change was observed in the tryptophan-rich C-terminal region of the sequence S-MPER (DKTLPDQGDNDNWWTGWRQW) upon binding with DPC micelles. Additionally, the MPER located in the gp41 of HIV is characterized by the presence of hydrophobic and aromatic residues, especially tryptophan, which are essential for viral entry, as demonstrated by alanine substitution of tryptophan [26,27].

Evidence also reported that the MPER region can induce antiviral immunity and is a target of broad-spectrum neutralizing antibodies. In line with this, we previously showed that a peptide belonging to FIV TM protein (LQKWEDWVRWIGNIPQYLKG), coupled with virus-like particles (VLPs) from the Qβ phage, is able to stimulate an humoral immune response in cats against the tryptophan-rich motif (TrpM) of FIV [28]. Turning to HIV, Huang *et* al. isolated and characterized a MPER-specific antibody, termed 10E8, which exerts potent viral neutralization. Interestingly, the same study reported that 27% of the patient sera tested contained anti-MPER neutralizing antibodies [29]. Building on these findings, we previously published a peptide derived from internal fusion peptide (IFP, now recognized as fusion peptide FP) region of the Spike glycoprotein in the case of SARS-CoV-2, named PN19, which showed a potent SARS-CoV-2 antiviral activity *in vitro* ($IC_{50} = 0.20$ μM) interacting with the MPER derived peptide [Cys^{1196}]Spike(1196-1220) (CLIDLQELGKYEQYIKWPWYIWLGF) with a $K_d = 9.44$ nM, evaluated via Surface Plasmon Resonance (SPR) [30].

Based on the evidence reported above, we herein propose the synthesis, structural characterization and SARS-CoV-2 antiviral activity of several peptides derived from the sequence Spike(1196-1220) (Entry No. **1** in Table 1), aiming at a possible structure-activity relationship (SAR), based on different aromatic intramolecular interactions between amino acid side chains.

2. Results and discussion

2.1. Peptide synthesis and biological activity

As reported above, the key interaction that brings the viral and cell membranes into close proximity for fusion and subsequent cell entry is the formation of a 6-HB between HR1 and HR2. However, the final viral cell-fusion does not involve solely this intramolecular protein-protein interaction (PPI) but is also mediated by the IFP and MPER sequences. These regions are characterized by a high number of aromatic side chains, such as phenylalanine, tyrosine, and tryptophan, which participate in this interaction. We previously demonstrated that alanine substitution of aromatic residues in PN19 dramatically decreases both antiviral activity and affinity for [Cys^{1196}]Spike(1196-1220) [30]. The MPER region is a tryptophan-rich motif also found in other viruses that share SARS-CoV-2's viral entry mechanism [23,25,31].

With the aim of exploring the antiviral activity of the MPER region, we first synthesized the peptide Spike(1196-1220) (**1**) by induction-assisted solid-phase peptide synthesis (IA-SPPS). This sequence (SLIDLQELGKYEQYIKWPWYIWLGF) features a hydrophilic N-terminus and a strongly hydrophobic, aromatic-rich C-terminus. The latter is presumed to play an essential role in interacting with IFP. A series of N-

Table 1
MPER-derived peptides synthesized, the corresponding inhibitory activity [IC_{50} (mean ± SD) μM] and cytotoxicity [CC_{50} (mean ± SD) μM], and the content of helicity expressed as *R*-values (calculated as the ratio between the minima measured at 220 and 208 nm via CD spectroscopy).

No.	*Peptide*	*Sequence*	*IC_{50} (μM)*	*CC_{50} (μM)*	*R-value*[a] *(%)*
1	Spike(1196-1220)	Ac-SLIDLQELGKYEQYIKWPWYIWLGF-NH_2	1.92 ± 0.67	>100	67
2	Spike(1198-1220)	Ac-IDLQELGKYEQYIKWPWYIWLGF-NH_2	1.10 ± 0.21	>100	68
3	Spike(1200-1220)	Ac-LQELGKYEQYIKWPWYIWLGF-NH_2	0.99 ± 0.71	>100	59
4	Spike(1202-1220)	Ac-ELGKYEQYIKWPWYIWLGF-NH_2	0.40 ± 0.31	52 ± 8	58
5	Spike(1204-1220)	Ac-GKYEQYIKWPWYIWLGF-NH_2	0.08 ± 0.07	>100	53
6	Spike(1206-1220)	Ac-YEQYIKWPWYIWLGF-NH_2	0.11 ± 0.05	84 ± 11	51
7	Spike(1208-1220)	Ac-QYIKWPWYIWLGF-NH_2	0.94 ± 0.48	>100	48
8	Spike(1210-1220)	Ac-IKWPWYIWLGF-NH_2	0.40 ± 0.13	>100	48
9	Spike(1212-1220)	Ac-WPWYIWLGF-NH_2	0.03 ± 0.02	>100	>100
10	Spike(1214-1220)	Ac-WYIWLGF-NH_2	5.47 ± 1.02	>100	38
11	Spike(1212-1218)	Ac-WPWYIWL-NH_2	20.08 ± 9.01	>100	-
12	Spike(1196-1211)	Ac-SLIDLQELGKYEQYIK-NH_2	40.90 ± 7.40	>100	76
13	Scramble Spike(1204-1220)	Ac-WKFQYGPWGIIWLYKEY-NH_2	45.92 ± 7.56	>100	-
14	[$Ala^{1212,1214,1217}$]Spike(1212-1220)	Ac-APAYIALGF-NH_2	4.68 ± 1.34	82 ± 10	65
15	[Cys^{891}]Spike(861-891)	Ac-LPPLLTDEMIAQYTSALLAGTITSGWTFGAC-NH_2	-	-	-

[a] Peptides Spike(1212-1218) (peptide 11) and Spike(1204-1220) (peptide 13) are not listed because they display a random-coil conformation.

terminally shortened sequences of Spike(1196-1220) (**1**) were then prepared by IA-SPPS, continuing until the first tryptophan was deleted, yielding the peptide Spike(1214-1220) (**10**, Table 1).

The antiviral activity of the peptides listed in Table 1 was evaluated against SARS-CoV-2 in Vero E6 cells using an inhibitory viral plaque reduction assay (PRA). As shown in Table 1, the parent peptide Spike (1196-1220) **(1)** exhibited promising *in vitro* antiviral activity with an $IC_{50} = 1.92 \pm 0.67$ μM, which is approximately 10-fold higher than that of the previously studied sequence PN19 (peptide derived from the IFP region) [24]. Deletion of the N-terminal Ser-Leu dipeptide leading to Spike(1198-1220) (**2**) increased the antiviral activity by 2-fold. Continued removal of N-terminal residues yielded progressively more potent sequences, culminating in the heptadecapeptide Spike (1204-1220) (**5**, $IC_{50} = 0.08 \pm 0.07$ μM). A decrease in antiviral activity was then observed upon removal of tyrosine 1206 and tyrosine 1209 [Spike(1210-1220) (**8**), $IC_{50} = 0.40 \pm 0.13$ μM]. Conversely, the peptide Spike(1212-1220) (**9**), which contains a high density of aromatic residues, showed the highest activity in the series, with a nanomolar IC_{50} (0.03 ± 0.02 μM). As expected, removal of Trp 1212 dramatically increased the IC_{50} by a factor of 200. Finally, cytotoxicity was assessed by MTT reduction assay in Vero E6 cells, indicating that all peptides were non-toxic at concentrations corresponding to their IC_{50} values (Table 1); however, sequences Spike(1202-1220) (**4**) and Spike (1206-1220) (**6**) showed cytotoxicity at higher concentrations ($CC_{50} \approx 52$ μM and $CC_{50} \approx 84$ μM, respectively).

These results overall suggest that the N-terminal hydrophilic residues can interfere with the MPER-IFP interaction, providing a polar surface, which destabilizes aromatic/hydrophobic non-covalent binding between the two spike protein regions. Conversely, the tryptophan-rich C-terminal segment of Spike(1196-1220) (**1**) is the key motif for antiviral activity, with tryptophan residues being particularly important. To support this hypothesis, we synthesized both the peptide Spike(1196-1211) (**12**), corresponding to the N-terminal portion of Spike(1196-1220) (**1**), and [$Ala^{1212,1214,1217}$]Spike(1212-1220) (**14**), a version of Spike(1212-1220) (**9**) in which all tryptophan residues were substituted with alanine (Table 1). As indicated in Table 1, these analogs displayed minimal or no antiviral activity, with IC_{50} values above 20 μM, with peptide [$Ala^{1212,1214,1217}$]Spike(1212-1220) (**14**) showing marginal cytotoxicity. Furthermore, to demonstrate that the specific amino acid sequence is critical for activity, we designed the scrambled peptide Scramble Spike(1204-1220) (**13**), which displayed no antiviral activity ($IC_{50} = 45.92 \pm 7.56$ μM). In this context, we selected the analogue Spike(1204-1220) (**5**) as a model because scrambling the substantially shorter Spike(1212-1220) (**9**) might still yield an active peptide due to its limited length and similar residue composition. Finally, subsequent attempts to shorten Spike(1212-1220) (**9**) from the C-terminus resulted in the peptide Spike(1212-1218) (**11**), which was about 150-fold less active (Table 1). Additionally, peptides Spike(1204-1220) (**5**) and Spike (1212-1220) (**9**), featuring higher antiviral activity, were also tested against different SARS-CoV-2 variants. As reported in Table 2, these peptides maintain a high effectiveness among the different variants used. Conversely, peptide Scramble Spike(1204-1220) (**13**) confirms its inefficacy. Finally, we conducted a time-of-addition experiment with the peptide Spike(1212-1220) (**9**) to test the time course of the antiviral activity of this peptide. Table 2 shows that the addition of peptide Spike (1212-1220) (**9**) 1 h after SARS-CoV-2 infection significantly reduced antiviral activity (IC_{50} 0.09 vs 84 μM).

2.2. Analysis of α-helicity in MPER-derived peptides by CD spectroscopy

To evaluate the secondary structure propensity of the synthesized peptides, we employed circular dichroism (CD) spectroscopy, recording the spectra both in 1% TFE in phosphate buffer (PB) and 50% TFE in PB (Fig. 1, S29). In 1% TFE, all peptides showed spectra of a predominantly random-coil conformation (Figure S29). Upon increasing the TFE concentration to 50%, a stabilizing effect on peptide conformation was observed, in agreement with previous studies [32,33]. Under these conditions, most MPER-derived sequences adopted an α-helical secondary structure, characterized by the canonical double minima at 208 nm and 222 nm, except for Spike(1212-1218) (**11**) and Scramble Spike(1204-1220) (**13**), which still remain random-coils. *R*-values of the peptides in 50% TFE in PB are reported in Table 1, obtained as the ratio in ellipticity at wavelengths of 208 nm and 222 nm, which is a well-established approximation of the content of helicity [34]. Interestingly, a clear trend emerged from the truncation of the parent peptide Spike(1196-1220) (**1**). Progressive shortening from the N-terminus led to a decrease in the *R*-value, from 67% for Spike(1196-1220) (**1**) to 48% for Spike(1210-1220) (**8**). This trend supports the idea that the α-helical conformation of Spike(1196-1220) (**1**) is localized primarily within its N-terminal region. Focusing on the helical penalties of the different amino acids, the N-terminal region is rich in helix-inducing residues like glutamate, leucine, and lysine, whereas the highly aromatic C-terminal region consists mostly of amino acids with high helical penalties [35]. Indeed, the peptide Spike(1196-1211) (**12**), which is the N-terminal portion, exhibited a well-defined CD spectrum with strong α-helical character, with an *R*-value of 75%. Notably, the *R*-value increases to 65% in case of the alanine-substituted derivative [$Ala^{1212,1214,1217}$]Spike (1212-1220) (**14**), as expected, since the alanine is the best α-helix forming residue with the lowest α-helical penalty (0 kcal/mol) [35].

Focusing on the CD spectra of Spike(1212-1220) (**9**) and Spike(1214-1220) (**10**), the latter exhibits a random-coil conformation in 1% TFE (Fig. 1A), as reported for all the longer peptides, while the former tends to adopt an α-helical conformation. In this case, the CD profile shows a clear minimum at 208 nm, whereas the other is redshifted, likely due to distortion caused by the tryptophan residues [36]. Likewise, in 50% TFE, Spike(1212-1220) (**9**) adopted an α-helical structure (Fig. 1B). Interestingly, the calculated *R*-value for Spike(1212-1220) (**9**) exceeded 100%, a result attributed to the ellipticity minimum at 222 nm being lower than that at 208 nm. This spectral distortion may arise from an additional negative CD contribution, such as that generated by the stacking of aromatic side chains, which typically produces a characteristic positive band near 217 nm and a negative band near 227 nm [36]. In comparison, the shorter peptide Spike(1214-1220) (**10**) displays only a weak propensity for α-helix formation under the same conditions, with an *R*-value of 38% (Table 1).

Table 2
Effect of virus variant and varying time of peptide administration on MPER peptide inhibitory activity.

Peptide	SARS-CoV-2 variant IC_{50} (μM)			Time of addition relative to SARS-CoV-2 infection IC_{50} (μM)[a]			
	Pango lineage B.1	Delta-like pango lineage B.1.617.2	Omicron-like pango lineage BA.1	T-1	T0	T1	T2
Spike(1212-1220) (**9**)	0.09 ± 0.08	0.06 ± 0.05	0.04 ± 0.03	0.10 ± 0.11	0.09 ± 0.04	74.11 ± 34.2	>100
Spike(1204-1220) (**5**)	0.21 ± 0.11	0.11 ± 0.09	0.31 ± 0.22	Nd	Nd	Nd	Nd
Scramble Spike(1204-1220) (**13**)	>100	>100	>100	Nd	Nd	Nd	Nd

[a] SARS-CoV-2 infection of Vero E6 cells at MOI of 0.01 in presence of peptide added at the indicated time (h) relative to the infection. IC_{50}, 50% inhibitory activity (mean ± SD); Nd, not determined.

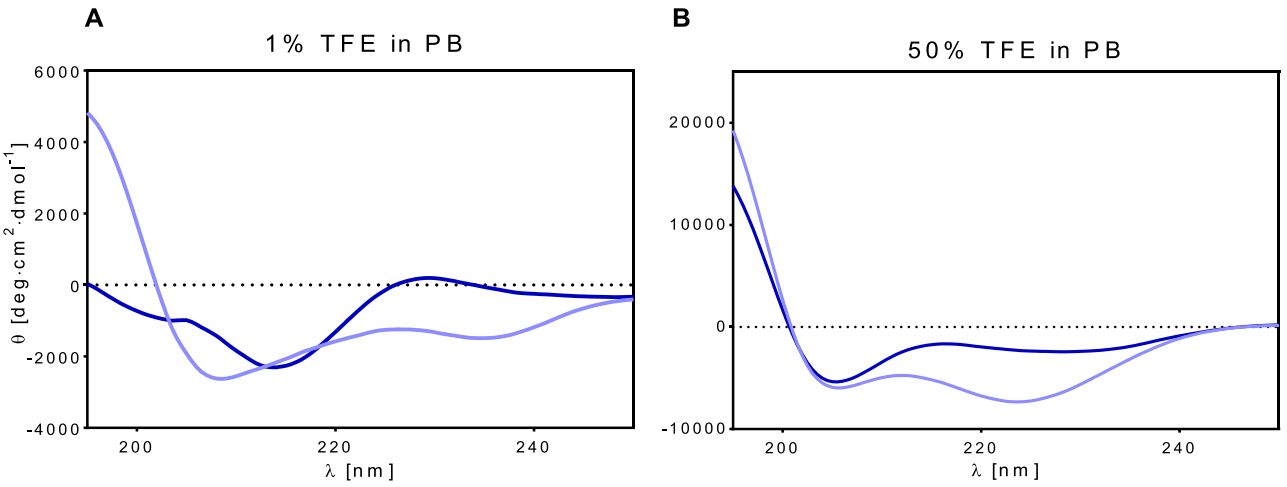

Fig. 1. Comparative analysis of CD spectra of Spike(1212-1220) (**9**, light blue) and Spike(1214-1220) (**10,** blue) in (A) 1% TFE in PB and (B) 50% TFE in PB.

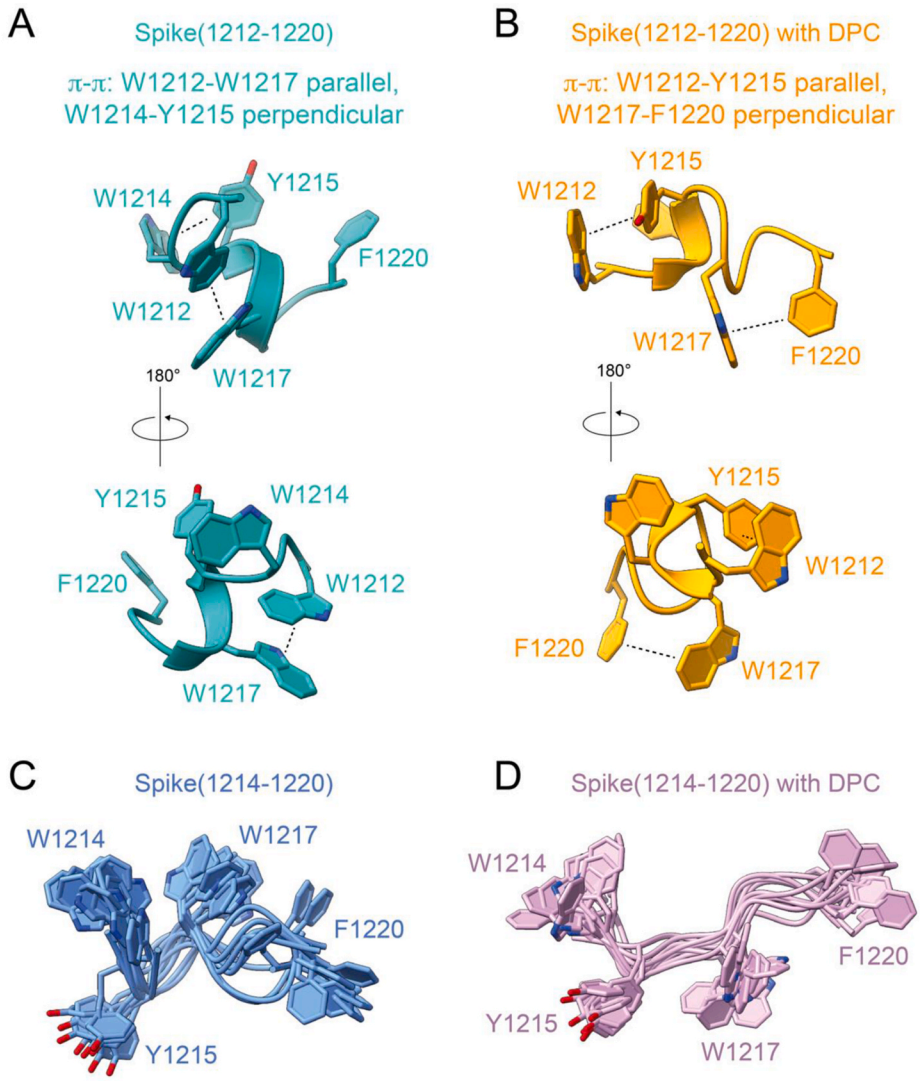

Fig. 2. NMR-derived structures of Spike(1212-1220) (**9**) in DMSO/H_2O (A) without n-dodecylphosphocholine (DPC) (green) and (B) in presence of DPC (orange). Parallel and perpendicular π-π interactions between aromatic amino acid side chains are indicated by dashed lines. Conformational ensembles of the ten lowest energy states as determined by NMR spectroscopy of Spike(1214-1220) (**10**) in DMSO/H_2O (C) without DPC (blue) and (D) in presence of DPC (magenta). Amino acids are abbreviated using one-letter code.

2.3. High resolution structural analysis of Spike(1212-1220) and Spike (1214-1220) by NMR spectroscopy

To gain insight into potential mode of action of the most potent peptide, Spike(1212-1220) (**9**), we sought to determine its high-resolution structure by NMR spectroscopy and compare it with that of Spike(1214-1220) (**10**) which showed significantly lower activity despite only missing two residues (tryptophan 1212 and proline 1213) (Table 1). As already indicated by CD spectroscopy, we expected that Spike(1212-1220) (**9**) features an α-helical structure (Fig. 1A). Indeed, we observe a well-defined α-helical conformation of this peptide by NMR spectroscopy measured in DMSO/H_2O (Fig. 2A).

Interestingly, aromatic side chains establish a distinct pattern of π-π interactions involving tryptophan and tyrosine residues. In Spike(1212-1220) (**9**) measured in DMSO/H_2O, these amino acids are tryptophan 1212, tryptophan 1214, tyrosine 1215 and tryptophan 1217 (Fig. 2A). In this structure, the indole moieties of the tryptophan 1212 and tryptophan 1217 side chains are oriented to one another in a parallel fashion, based on a classic planar π-π stacking mode of the aromatic heterocycles with bicyclic structure. The non-covalent interaction of tryptophan 1214 and tyrosine 1215, however, is based on perpendicular stacking, also known as T-shaped or edge-to-face interaction [37]. This type of π-π stacking is an attractive, non-covalent interaction where the electropositive hydrogen atoms on the edge of one aromatic ring (here tyrosine 1215) are directed toward the electronegative electron cloud of another aromatic ring (tryptophan 1214). In line with this, the hydroxyl group of tyrosine 1215 is oriented in opposite direction of the tryptophan 1214 indole moiety. Phenylalanine 1220 does not take part in these π-π interactions as its side chain is more than 6 Å away from the tyrosine 1215 phenol. These distinct π-π stacking modes may stabilize the observed α-helical structure of Spike(1212-1220) (**9**), which is in well agreement with the observation by CD spectroscopy where we detected an α-helical contribution and even indication of stacking of aromatic side chains (Fig. 1A and B).

As we designed the MPER-derived peptides with the idea to target the membrane-associated regions of SARS-CoV-2 spike protein subunit S2 involved in the viral cell fusion step, we investigated the structure of Spike(1212-1220) (**9**) in context of micelles based on *n*-dodecylphosphocholine (DPC), which is a well-established system for structural and biophysical studies of membrane proteins and binding of peptides to membranes [38,39]. The structure of Spike(1212-1220) (**9**) in presence of DPC micelles determined by NMR highlights again an α-helical structure, with somewhat distorted backbone conformation relative to the structure without DPC (Fig. 2B). This structural change is most likely induced by a different π-π stacking pattern due to interactions with the micelles. Now, in presence of DPC, the side chains of tryptophan 1212 and tyrosine 1215 orient parallel to each other, whereas the indole moiety of tryptophan 1217 interacts perpendicular with the benzene ring of phenylalanine 1220 (Fig. 2B). Further solid-state NMR-based studies employing magic-angle-spinning (MAS) of Spike(1212-1220) (**9**) in context of lipid bilayers may provide valuable insight into the relevance of lipids toward biological activity of the peptide.

To find reason why Spike(1212-1220) (**9**) has about 180-fold higher antiviral activity than peptide Spike(1214-1220) (**10**), which only lacks one tryptophan and one proline residue at the N-terminus, we also determined the high-resolution structure of Spike(1214-1220) (**10**) by NMR (Fig. 2C). In DMSO/H_2O, this peptide shows high structural variability as the ten lowest energy states do not converge to a well-defined conformational ensemble but feature much higher flexibility. Even though a tendency towards α-helical conformation may be present, no π-π stacking of aromatic side chains is observed in contrast to Spike (1212-1220) (**9**). The same observation is made in the NMR structure of this shortened peptide in presence of DPC micelles (Fig. 2D). This indicates a correlation between α-helical structure of the peptide Spike (1212-1220) (**9**), induced by aromatic side chain stacking, and high antiviral activity. As Spike(1214-1220) (**10**) lacks tryptophan 1212, it further suggests that tryptophan 1212 is a key residue and essential to establish the π-π interaction pattern to form an α-helical structure. The potential role of proline 1213, however, cannot be excluded based on these data.

2.4. Structural comparison of Spike(1212-1220) and SARS-CoV-2 spike subunit S2 indicates potential mode of action based on competition

As the presented peptides are derived from the transmembrane anchor (TM) segment of the SARS-CoV-2 spike subunit S2, we hypothesized that Spike(1212-1220) (**9**) may compete with the viral protein domains involved in protein-protein interaction in lipid context and thus block membrane fusion, resulting in antiviral activity. To analyze whether such competition is conceivable, we modeled the NMR-derived Spike(1212-1220) (**9**) structure presented here into the SARS-CoV-2 spike subunit S2 structure solved recently by cryo-electron microscopy (cryo-EM) (Fig. 3) (pdb code 8FDW) [40]. This structure of SARS-CoV-2 spike subunit S2 shows that the TM segment of one protomer interacts with the FP region of another protomer to establish the post-fusion structure, and the TM, FP and FP proximal region (FPPR) segments are involved in interaction with the host cell membrane as suggested by the cryo-EM structure in nanodiscs (Fig. 3A). In SARS-CoV-2 spike

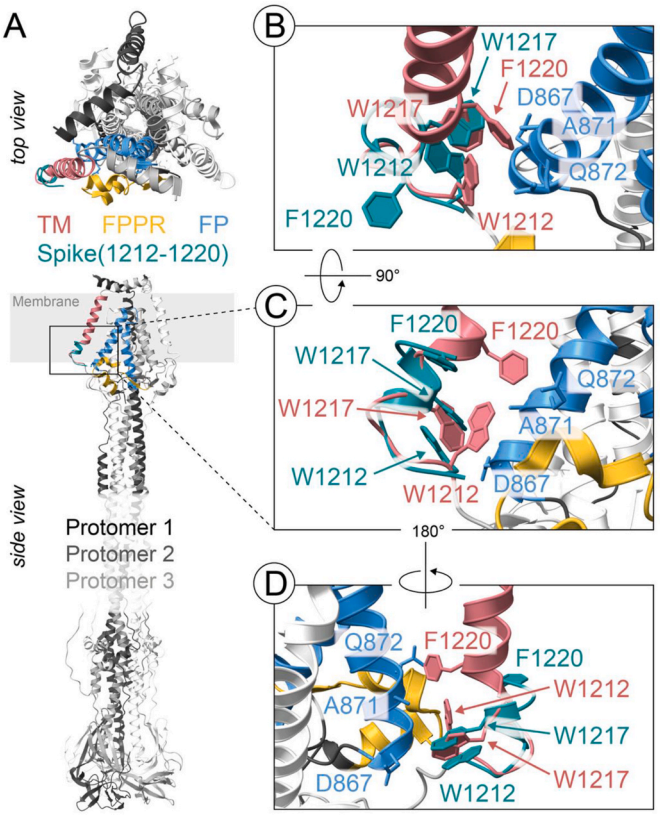

Fig. 3. Structural analysis of potential mode of action of Spike(1212-1220) (**9**). (A) The NMR-derived structure of Spike(1212-1220) (**9**) (green) is superimposed with the structural model of the trimeric SARS-CoV-2 spike protein as determined by cryo-electron microscopy (pdb code 8FDW) [40]. The backbone conformation of Spike(1212-1220) (**9**) matches the N-terminal part of the transmembrane anchor (TM) segment (red) of the spike protein. The fusion peptide (FP, blue) and FP proximal region (FPPR, yellow) segments of the SARS-CoV-2 spike protein are involved in membrane binding. (B), (C) and (D) Amino acid residues involved in interaction of TM (red) and FP (blue) are highlighted as proposed by the cryo-EM structure. Deviations in amino acid side chain orientations between Spike(1212-1220) (**9**) (green) and TM (red) of the SARS-CoV-2 spike protein are discussed in the main text. Amino acids are abbreviated using one-letter code.

subunit S2, residues critically involved in this protein-protein interaction are tryptophan 1212 and 1217, which establish the aromatic stacking observed in the peptide Spike(1212-1220) (**9**) resulting in its α-helical structure, and phenylalanine 1220. The cryo-EM structure indicates further that aspartate 867, alanine 871 and glutamine 872 in FP are interaction partners to the TM segment (Fig. 3B–D) [40]. We hypothesize that peptide Spike(1212-1220) (**9**) may interact with the spike protein near the FP region, thus interfering with the subsequent molecular event of 6-HB formation. This supposed mode of action may involve a possible competition role of the peptide after 6-HB formation, perturbing the interaction of the subunit S2 MPER and FP domains and with lipids of the host cell membrane, thus blocking or slowing down the membrane fusion process. If an interaction between Spike(1212-1220) (**9**) and the FP region of the spike protein occurs, it is well conceivable that it happens in a stepwise manner, essentially successively binding to the different protomers. Spike(1212-1220) (**9**) is prone to form oligomers and aggregates in aqueous solution and may thus bind to FP regions of different protomers of the protein available before fusion of the spike.

In this model presented here, the Spike(1212-1220) (**9**) structure superimposes well with the N-terminal part of the TM segment of the SARS-CoV-2 spike protein subunit S2 (Fig. 3). Residues tryptophan 1212 and tryptophan 1217 feature backbone conformations that match those of the SARS-CoV-2 spike protein, with small deviations in the side chain orientations. These may result from different sample conditions as we measured the NMR data of the peptide in DMSO/H_2O mixture, whereas the cryo-EM data of the spike protein were collected in the post-fusion state in nanodiscs [40]. This may also explain the large deviation in conformation of phenylalanine 1220 between Spike(1212-1220) (**9**) and SARS-CoV-2 spike protein (Fig. 3B–D). The observed differences in peptide conformation and aromatic stacking involving phenylalanine 1220 between the DPC micelle-bound and DPC micelle-free states points towards a significant role of lipids in establishing the functionally relevant conformation of Spike(1212-1220) (**9**) to compete with SARS-CoV-2 spike protein in membrane binding (Fig. 2). Another striking difference between the Spike(1212-1220) (**9**) and SARS-CoV-2 spike protein structures is the different aromatic π-π stacking modes of the tryptophan 1212 and 1217 side chains (parallel in Spike(1212-1220) (**9**), perpendicular in SARS-CoV-2 spike protein) (Fig. 3D). In addition to the structural differences in phenylalanine 1220, this may be a promising feature to address to enhance antiviral potency of the peptide. More detailed investigations either employing lipid bilayers or membranes and solid-state MAS NMR, or nanodisc-based samples in solution-state NMR, may shed light onto this mechanistically important question and help to further improve the efficacy. Since Spike (1212-1220) (**9**) mimics the conformation of the N-terminal part of the TM segment in the full-length protein in general very well, it may bind to the cognate FP region as shown in the post-fusion structure of the protein by cryo-EM and thereby block the fusion. As mentioned in the introduction, we have previously presented an IFP peptide of SARS-CoV-2 (PN19), which showed a potent antiviral activity *in vitro* ($IC_{50} = 0.20$ μM) and interacts with the MPER-derived peptide [Cys^{1196}] Spike(1196-1220) (CLIDLQELGKYEQYIKWPWYIWLGF) with a $K_d = 9.44$ nM, as determined by Surface Plasmon Resonance (SPR) [30]. To further validate the idea that MPER sequences bind to the FP region, we performed SPR binding measurements by inverting the ligand and analyte configurations. Specifically, the FP-derived peptide [Cys^{891}] Spike(861-891) (**15**) was covalently immobilized onto the gold surface of the SPR sensor chip, while the different MPER peptides were injected as analytes. As shown in the histogram below (Fig. 4), the longest peptide, Spike(1196-1220) (**1**), successfully interacts with the immobilized FP fragment. Notably, the shorter sequences Spike(1208-1220) (**7**) and Spike(1210-1220) (**8**) exhibited a stronger binding response, mirroring their higher antiviral activity. However, peptide Spike(1212-1220) (**9**) did not yield any signal. This lack of interaction might be attributed to peptide aggregation, triggered by its high content of aromatic residues.

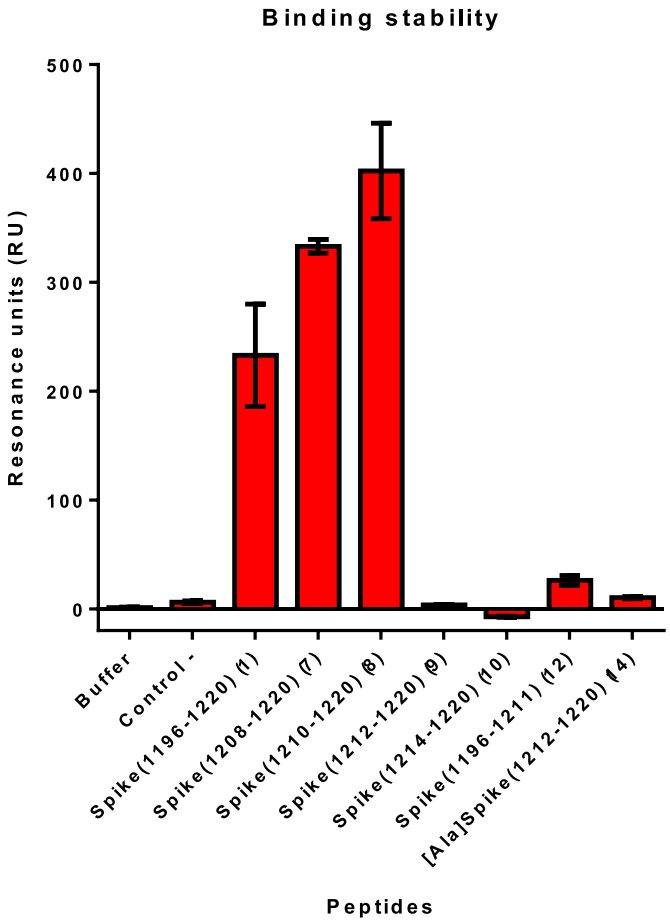

Fig. 4. [Cys^{1196}]Spike(1196-1220) SPR binding activity of MPER peptides. Binding levels to immobilized [Cys^{1196}]Spike(1196-1220) peptide of peptides Spike(1196-1220) (**1**), Spike(1208-1220) (**7**), Spike(1210-1220) (**8**), Spike (1212-1220) (**9**), Spike(1214-1220) (**10**), Spike(1196-1211) (**12**), and [$Ala^{1212,1214,1217}$]Spike(1212-1220) (**14**) at the concentration 100 μM. Peptide [Cys^{1196}]Spike(1196-1220) was covalently immobilized onto the gold surface of the biosensor following the thiol coupling immobilization strategy. All peptides were flowed separately over the immobilized [Cys^{1196}]Spike(1196-1220) fragment in individual cycle of analysis with an initial association phase (sample injection), a second dissociation phase (washing step with running buffer), and finally a chip surface regeneration phase. Background levels due to non-specific peptide interactions were monitored on the reference channel of the chip and subtracted from sample signals. The running buffer and a control peptide have been also tested as negative controls. [Ala]Spike(1212-1220) (**14**) refers to [$Ala^{1212,1214,1217}$]Spike(1212-1220) (**14**).

Consequently, the presence of the Lys residue in Spike(1210-1220) (**8**) likely improves solubility, preventing such self-association. Finally, the less active sequence Spike(1196-1211) (**12**), and sequences Spike (1214-1220) (**10**) and [$Ala^{1212,1214,1217}$]Spike(1212-1220) (**14**) showed no significant binding. Taking together, these results confirm that the antiviral activity of the peptides listed in Table 1 correlates with their ability to bind the target FP region.

3. Conclusions

In this study, we investigated MPER-derived peptides from the SARS-CoV-2 spike protein and identified short aromatic-rich sequences with potent antiviral activity against different SARS-CoV-2 variants. Systematic truncation revealed that peptides containing clustered tryptophan and tyrosine residues exhibit the strongest inhibition of viral infection. Moreover, such activity was time-depended, exhibiting a great reduction when peptide was added 1 h after infection. NMR structural

analysis demonstrated that these peptides form a well-defined α-helix in solution and DPC-based micelles that is stabilized by intramolecular aromatic π-π stacking interactions. This aromatic network appears to pre-organize the peptide structure and likely promotes interactions with the viral fusion machinery at the membrane interface. The strong correlation between aromatic residue content, helix stability, and antiviral potency highlights π-stacking as a key determinant of antiviral activity, as already observed with several viruses, such as SARS-CoV, HIV, FIV and EBOV [22–24,41]. To date, structural and functional evidences strongly support an interplay between the S2 HR1 and HR2 subunits in SARS-CoV-2 fusion process, as observed in other viruses [42]. In this context, owing to their aromatic-rich motif, interactions between the MPER and the fusion peptide appear to play a key role in driving the viral membrane fusion event. Our findings indicate that the SARS-CoV-2 MPER peptide **9** reproduces the endogenous Spike region in the post-fusion structure and, thanks to the presence of tryptophan residues stabilizing its conformation, exhibits strong antiviral activity. Although the therapeutic use of small peptides is limited due to their low bioavailability, the results presented here provide further molecular insights into the functional role of the MPER region in viral entry and could serve as a springboard for the design and development of biologically more stable peptide and peptidomimetics inhibitors targeting coronavirus membrane fusion [43].

4. Experimental section

4.1. Reagents

All Fmoc-protected amino acids, *N,N′*-diisopropylcarbodiimide (DIC), OxymaPure® (ethyl cyanohydroxyiminoacetate) were purchased from Iris Biotech GmbH (Marktredwitz, Germany). Tentagel® S RAM resin was purchased from Rapp Polymere (Tuebingen, Germany). Peptide-synthesis grade *N,N*-dimethylformamide (DMF) and acetonitrile (ACN) were purchased from Carlo Erba (Milano, Italy). Dichloromethane (DCM), trifluoroacetic acid (TFA), triisopropylsilane (TIS), acetic anhydride (Ac_2O), and piperidine were purchased from Sigma-Aldrich (Milano, Italy). Surface plasmon resonance experiments were performed in a Biacore® X100 instrument from Cytiva™ (Uppsala, Sweden). All solutions were prepared with Milli-Q water obtained using the Sartorius system (Arium® 611 VF), which were filtered daily with a Millipore Express™ PLUS 0.22 μm filtration system. The CM5-type chips, amine coupling kit, 10 mM pH 2.5 glycine solution, and running buffer HBS-EP+ 10× (0.1 M HEPES, 1.5 M NaCl, 30 mM EDTA, 0.5% v/v surfactant P20) were purchased by Cytiva™ (Uppsala, Sweden). Running buffer was diluted ten times with Milli-Q water at pH 7.4 and filtered daily.

4.2. Peptide synthesis

The MPER peptides were synthesized by Induction-assisted Solid-Phase Peptide Synthesis (I-SPPS) following the Fmoc/*t*Bu orthogonal protection strategy, using the PurePep™Chorus™ automated peptide synthesizer (Gyros Protein Technologies, Uppsala, Sweden). Tentagel® S RAM resin was used (loading 0.23 mmol/g). The following Fmoc-L-amino acids were used: Fmoc-Ala-OH, Fmoc-Cys(Trt)-OH, Fmoc-Asp(O*t*Bu)-OH, Fmoc-Glu(O*t*Bu)-OH, Fmoc-Phe-OH, Fmoc-Gly-OH, Fmoc-Ile-OH, Fmoc-Lys(Boc)-OH, Fmoc-Leu-OH, Fmoc-Pro-OH, Fmoc-L-Gln(Trt)-OH, Fmoc-Ser(*t*Bu)-OH, Fmoc-Trp(Boc)-OH, Fmoc-Tyr(*t*Bu)-OH. Fmoc deprotections were performed with a solution of 20% piperidine in DMF for 60 s at 90 °C. Peptide assembly was performed by repeating the SPPS standard coupling cycle for each amino acid, using Fmoc-protected amino acids (5 eq.), OxymaPure® (5 eq.), and DIC (5 eq.) dissolved in DMF for 120 s at 90 °C. The washing steps were performed using a mixture of EtOAc/DMSO 8:2 (*v/v*). The N-acetylation was performed using a solution of 10% Ac_2O in DMF for 4 min at 40 °C. Final cleavage and side-chain deprotections were performed using a mixture of TFA/TIS/H_2O (95:2.5:2.5, *v/v/v*) at r.t. After 3 h the resin was filtered off. The peptide was precipitated with cold mixture 1:1 Et_2O/hexanes (*v/v*), centrifuged, and lyophilized. In case of the presence of carbamate moieties attached to the Trp residues as incomplete deprotection, the crude peptide was further treated with few drops of 1 M HCl for 2 h at r.t and lyophilized. In the case of Spike(1212-1220) (**9**), Spike(1214-1220) (**10**) and Spike(1212-1218) (**11**) peptides, Fmoc-Trp-OH without side-chain protection was used, to avoid harsh conditions to remove the carbamate moieties.

Table 3
Gradients for the MPER-derived analogs and [Cys^{891}]Spike(861-891) purification using an AquaC18 column (Phenomenex, Torrance, USA) (5 μm, 250 × 10 mm), at 4 mL/min with solvent systems A (0.1% TFA in H_2O) and B (0.1% TFA in ACN) over 30 min.

No.	Peptide	Gradient (% B)
1	Spike(1196-1220)	35 - 90
2	Spike(1198-1220)	35 - 90
3	Spike(1200-1220)	35 - 90
4	Spike(1202-1220)	35 - 90
5	Spike(1204-1220)	35 - 90
6	Spike(1206-1220)	35 - 90
7	Spike(1208-1220)	35 - 90
8	Spike(1210-1220)	35 - 90
9	Spike(1212-1220)	35 - 90
10	Spike(1214-1220)	35 - 90
11	Spike(1212-1218)	25 - 90
12	Spike(1196-1211)	35 - 90
13	Spike(1204-1220)s	25 - 90
14	[$Ala^{1212,1214,1217}$]Spike(1212-1220)	25 - 90
15	[Cys^{891}]Spike(861-891)	40 - 95

4.3. Peptide purification and characterization

The crude peptides were purified by semipreparative RP-HPLC on a Waters instrument (Separation Module 2695, detector diode array 2996) using an AquaC18 column (Phenomenex, Torrance, USA) (5 μm, 250 × 10 mm), at 4 mL/min with solvent systems A (0.1% TFA in H_2O) and B (0.1% TFA in ACN) using the gradients reported in Table 3 over 30 min.

Analytical characterization of the MPER peptides was performed RP-HPLC Alliance Chromatography system (Waters, Milford Massachusetts, USA) coupled to a single quadrupole ESI-MS (Waters® ZQ Detector, Waters Milford, MA, USA) supplied with a Supelco BIOshell A160 Peptide C18 (2.7 μm 3.0 × 100 mm) column at 308 K, at 0.6 mL/min using solvent systems A (0.1% TFA in H_2O) and B (0.1% TFA in ACN). The analytical data, the chromatograms, and mass spectrometry spectra are reported in Table S1 and Figures S1 – S30.

4.4. Circular dichroism

CD spectra of the MPER peptides were recorded using quartz cells of 1 cm path length with a JASCO J-1500 CD spectropolarimeter (Tokyo, Japan) at 298 K. The conditions used were 1% TFE in PB and 50% TFE in PB at a concentration of 10 μM prepared from 500 μM stock solutions of the peptides dissolved in 1:1 TFE/H_2O. The specta were measured in the 250 - 195 nm spectral range, 1 nm bandwidth, 3 accumulations, and 50 nm/min scanning speed. The CD spectra of the synthesized peptides are reported in Figure S31.

4.5. NMR spectroscopy

NMR experiments were performed on a Bruker Avance III HDX 500 MHz NMR spectrometer equipped with a cryogenically cooled 5 mm $^{1}H/^{13}C/^{15}N$ TCI probe. The peptide sample (approximately 10 mg) was dissolved in a solution of DMSO-d_6/H_2O (80:20, v/v). For structural studies of peptide-micelle interactions, 10 mg peptide was dissolved in a

solution of DMSO-d_6/H_2O (80:20, v/v) and 50 mM *n*-dodeclyphosphocholine (DPC). All spectra were recorded at 303 K. Resonance assignments were achieved using a set of scalar coupling-based NMR spectra (^1H,^1H-TOCSY, ^1H,^{13}C-HSQC and ^1H,^{15}N-HSQC). Structures were calculated based on two-dimensional ^1H,^1H-NOESY experiments. ^1H,^1H-TOCSY experiments were recorded using WATERGATE solvent suppression with 300 ms and 32 scans, and 146 ms and 73 ms were aquired in the direct and indirect dimensions, respectively (spectral widths of 14 ppm in both dimensions were used). ^1H,^{13}C-HSQC spectra were acquired using WATERGATE with 128 scans. 146 ms were recorded in the ^1H-dimension at a spectral width of 14 ppm and 17 ms at a spectral width of 200 ppm in the ^{13}C-dimension. ^1H,^{15}N-HSQC experiments were recorded using water flip-back and WATERGATE with 1024 scans and 146 ms at a spectral width of 14 ppm in the ^1H-dimension and 31 ms at a spectral width of 40 ppm in the ^{15}N-dimension. ^1H,^1H-NOESY spectra were acquired with water flip-back and WATERGATE, 128 scans and a NOE mixing time of 300 ms, and 146 ms and 73 ms were aquired in the direct and indirect dimensions, respectively. Spectral widths of 14 ppm in both dimensions were used. All spectra were processed using TopSpin version 3.6 and analyzed using CCPNmr [44]. Structures were calculated using Artificial Intelligence for NMR Applications (ARTINA) on the NMRtist cloud computing service, employing FLYA automated chemical shift assignment and structure calculation with CYANA [45]. All observed chemical shifts and their assignments were checked manually and are listed in the Supporting Information (Tables S2 - S5).

4.6. Antiviral activity

The inhibitory activity against SARS-CoV-2 with selected MPER-derived peptides was performed in Vero E6 cells (BS-CCLO87, ATCC, Rockville, Md, USA) in 6-well plates using multiplicities of infection (MOI) of 0.01. Plaque reduction (PRA) activity peptides on viral replication were analyzed at 3 days compared to the viral control grown in absence of the peptides. Briefly, virus mixed with serial dilution (final concentration ranged from 0.1 to 100 μM) of peptide diluted in DMSO was inoculated on Vero E6 cell in presence of L-1-tosylamido-2-phenylethyl-chloromethyl-ketone-treated trypsin (2 μg/mL; Sigma, St. Louis, MO, USA) and incubated 1 h at 37 °C in humidified air with 5% CO_2 [46]. Virus mixed with DMSO alone was used as control of replication. Then, the cells underwent a 1X PBS wash before receiving a 0.5% Sea Plaque Agarose overlay in serum-free propagation medium and supplemented with L-1-tosylamido-2-phenylethyl-chloromethyl-ketone-treated trypsin (2 μg/mL; Sigma, St.Louis, MO, USA). Plaque reduction (PRA) was analyzed at 3 days compared to the viral control grown in absence of the peptides. 50% inhibitory concentrations (IC_{50}) were calculated using the predicted exponential growth function in Microsoft Excel.

4.7. Cell cytotoxicity assay

The cytotoxicity of peptides was evaluated by the MTT reduction assay. Vero E6 cells were plated at a density of 10^4 cells per well in a flat-bottom 96-well culture plate and allowed to adhere overnight. Then, the medium was removed, the wells were washed twice with PBS and treated with 100 μL of MEM alone or with or without the appropriate concentrations of the peptides (final concentrations ranged from 0.1 to 100 μM) and incubated at 37 °C in a CO_2 incubator for 72 h. After treatment, an MTT kit (Roche, Milan, Italy) was used according to the supplier's instructions, and the absorbance of each well was determined using a microplate spectrophotometer at a wavelength of 595 nm. Cytotoxicity was calculated by dividing the average optical density of treated samples by the average of the mock-treated samples in the presence of DMSO alone.

4.8. Surface plasmon resonance assay

The peptide [Cys^{891}]Spike(861-891) (**15**) was immobilized following the standard surface thiol coupling strategy on a sensor chip CM5-type. At this purpose, immobilization buffer was previously selected using the pH scouting protocol, identifying the 20 mM acetate buffer at pH 4.5 as optimal buffer for immobilization. Then, sensor surface was activated by injecting a solution 0.4 M of 1-ethyl-3-[3-dimethylaminopropyl]carbodiimide (EDC) and 0.1 M of N-hydroxysuccinimide (NHS) (50:50) for 4 min at a flow rate of 10 μL/min. Then a solution of 80 mM 2-(2-pyridinyldithio)ethaneamine (PDEA) in 0.1 M sodium borate pH 8.5 used within 1 h of preparation was injected for 4 min at a flow rate of 10 μL/min. The peptide [Cys^{891}]Spike(861-891) (**15**) was then injected for 7 min at a flow rate of 10 μL/min, repeating this operation 10 times till raising an immobilization level of 1200 resonance units (RU) approximately. Deactivation of excess active groups on chip surface were performed by injecting a solution 50 mM L-cysteine and 1 M NaCl in 0.1 M sodium acetate at pH 4.0 for 4 min at a flow rate of 5 μL/min. In parallel, a reference channel on the chip surface was prepard by activating and then deactivating functional groups.

The peptides Spike(1196-1220) (**1**), Spike(1208-1220) (**7**), Spike (1210-1220) (**8**), Spike(1212-1220) (**9**), Spike(1214-1220) (**10**), Spike (1196-1211) (**12**), and [$Ala^{1212,1214,1217}$]Spike(1212-1220) (**14**) were flowed independently over the sensor chip surface at the final concentration of 100 μM for 120 s at a flow rate of 30 μL/min. Data were reported as resonance units (RU) obtained during the binding stability to peptide [Cys^{891}]Spike(861-891) (**15**) subtracting the signal of the reference channel.

CRediT authorship contribution statement

Michael Quagliata: Conceptualization, Data curation, Writing – original draft, Writing – review & editing. **Sonja Bazhenova:** Conceptualization, Writing – original draft. **Rosaria Arvia:** Conceptualization, Data curation, Writing – original draft. **Shima Siadohoni:** Conceptualization, Data curation. **Andrea Di Santo:** Conceptualization, Data curation. **Feliciana Real-Fernandez:** Formal analysis, Investigation. **Anna Maria Papini:** Conceptualization, Writing – review & editing. **Simone Giannecchini:** Conceptualization, Resources, Supervision, Writing – review & editing. **Daniel Friedrich:** Conceptualization, Data curation, Resources, Supervision, Writing – original draft, Writing – review & editing. **Paolo Rovero:** Conceptualization, Funding acquisition, Investigation, Supervision, Writing – review & editing.

Declaration of competing interest

The authors declare that they have no known competing financial interests or personal relationships that could have appeared to influence the work reported in this paper.

Acknowledgments

We are grateful to Ines Neundorf for initiating the collaboration that led to this work and for her valuable support throughout the study. We thank Daniela Naumann, Kathrin König and Philipp Hegemann for excellent maintenance of the NMR facility at University of Cologne. This work was supported by the German Research Foundation (DFG) [grant FR 4220/2-1] and institutional funding from the University of Cologne.

Appendix ASupplementary data

Supplementary data to this article can be found online at https://doi.org/10.1016/j.ejmech.2026.119122.

Data availability

Data will be made available on request.

References

[1] *COVID-19 cases | WHO COVID-19 dashboard.* datadot. https://data.who.int/dashboards/covid19/cases. (Accessed 1 November 2025).

[2] Commissioner, O. of the, FDA approves first COVID-19 vaccine. FDA. https://www.fda.gov/news-events/press-announcements/fda-approves-first-covid-19-vaccine. (Accessed 1 November 2025).

[3] M.J. Mulligan, K.E. Lyke, N. Kitchin, J. Absalon, A. Gurtman, S. Lockhart, K. Neuzil, V. Raabe, R. Bailey, K.A. Swanson, P. Li, K. Koury, W. Kalina, D. Cooper, C. Fontes-Garfias, P.-Y. Shi, Ö. Türeci, K.R. Tompkins, E.E. Walsh, R. Frenck, A. R. Falsey, P.R. Dormitzer, W.C. Gruber, U. Şahin, K.U. Jansen, Phase I/II study of COVID-19 RNA vaccine BNT162b1 in adults, Nature 586 (7830) (2020) 589–593, https://doi.org/10.1038/s41586-020-2639-4.

[4] Commissioner, O. of the, Coronavirus (COVID-19) update: FDA authorizes additional oral antiviral for treatment of COVID-19 in certain adults. FDA. https://www.fda.gov/news-events/press-announcements/coronavirus-covid-19-update-fda-authorizes-additional-oral-antiviral-treatment-covid-19-certain. (Accessed 1 November 2025).

[5] M. Toots, J.-J. Yoon, M. Hart, M.G. Natchus, G.R. Painter, R.K. Plemper, Quantitative efficacy paradigms of the influenza clinical drug candidate EIDD-2801 in the ferret model, Transl. Res. J. Lab. Clin. Med. 218 (2020) 16–28, https://doi.org/10.1016/j.trsl.2019.12.002.

[6] F. Messina, E. Giombini, C. Montaldo, A.A. Sharma, A. Zoccoli, R.-P. Sekaly, F. Locatelli, A. Zumla, M. Maeurer, M.R. Capobianchi, F.N. Lauria, G. Ippolito, Looking for pathways related to COVID-19: Confirmation of Pathogenic mechanisms by SARS-CoV-2–Host interactome, Cell Death Dis. 12 (8) (2021) 788, https://doi.org/10.1038/s41419-021-03881-8.

[7] W. Cao, C. Dong, S. Kim, D. Hou, W. Tai, L. Du, W. Im, X.F. Zhang, Biomechanical characterization of SARS-CoV-2 spike RBD and human ACE2 protein-protein interaction, Biophys. J. 120 (6) (2021) 1011–1019, https://doi.org/10.1016/j.bpj.2021.02.007.

[8] J.A. Jaimes, J.K. Millet, G.R. Whittaker, Proteolytic cleavage of the SARS-CoV-2 spike protein and the role of the novel S1/S2 site, iScience 23 (6) (2020) 101212, https://doi.org/10.1016/j.isci.2020.101212.

[9] C.B. Jackson, M. Farzan, B. Chen, H. Choe, Mechanisms of SARS-CoV-2 entry into cells, Nat. Rev. Mol. Cell Biol. 23 (1) (2022) 3–20, https://doi.org/10.1038/s41580-021-00418-x.

[10] T. Tang, M. Bidon, J.A. Jaimes, G.R. Whittaker, S. Daniel, Coronavirus membrane fusion mechanism offers a potential target for antiviral development, Antivir. Res. 178 (2020) 104792, https://doi.org/10.1016/j.antiviral.2020.104792.

[11] M. Quagliata, A.M. Papini, P. Rovero, Chemically modified antiviral peptides against SARS-CoV-2, J. Pept. Sci. 30 (2) (2024) e3541, https://doi.org/10.1002/psc.3541.

[12] M. Quagliata, M.A. Stincarelli, A.M. Papini, S. Giannecchini, P. Rovero, Antiviral activity against SARS-CoV-2 of conformationally constrained helical peptides derived from angiotensin-converting enzyme 2, ACS Omega 8 (25) (2023) 22665–22672, https://doi.org/10.1021/acsomega.3c01436.

[13] N. Düzgüneş, N. Fernandez-Fuentes, K. Konopka, Inhibition of viral membrane fusion by peptides and approaches to peptide design, Pathogens 10 (12) (2021) 1599, https://doi.org/10.3390/pathogens10121599.

[14] J. LaBonte, J. Lebbos, P. Enfuvirtide Kirkpatrick, Nat. Rev. Drug Discov. 2 (5) (2003) 345–346, https://doi.org/10.1038/nrd1091.

[15] A.G. Schmidt, P.L. Yang, S.C. Harrison, Peptide inhibitors of dengue-virus entry target a late-stage fusion intermediate, PLoS Pathog. 6 (4) (2010) e1000851, https://doi.org/10.1371/journal.ppat.1000851.

[16] M. Kandeel, M. Yamamoto, B.K. Park, A. Al-Taher, A. Watanabe, J. Gohda, Y. Kawaguchi, K. Oh-hashi, H.-J. Kwon, J. Inoue, Discovery of new potent Anti-MERS CoV fusion inhibitors, Front. Pharmacol. 12 (2021), https://doi.org/10.3389/fphar.2021.685161.

[17] K.S. Schmitz, D. Geers, R.D. de Vries, T.F. Bovier, A.Z. Mykytyn, C.H. Geurts van Kessel, B.L. Haagmans, M. Porotto, R.L. de Swart, A. Moscona, Potency of fusion-inhibitory lipopeptides against SARS-CoV-2 variants of concern, mBio 13 (3) (2022) e01249-22, https://doi.org/10.1128/mbio.01249-22.

[18] R.D. De Vries, K.S. Schmitz, F.T. Bovier, C. Predella, J. Khao, D. Noack, B. L. Haagmans, S. Herfst, K.N. Stearns, J. Drew-Bear, S. Biswas, B. Rockx, G. McGill, N.V. Dorrello, S.H. Gellman, C.A. Alabi, R.L. De Swart, A. Moscona, M. Porotto, Intranasal fusion inhibitory lipopeptide prevents direct-contact SARS-CoV-2 transmission in ferrets, Science 371 (6536) (2021) 1379–1382, https://doi.org/10.1126/science.abf4896.

[19] S. Mougari, V. Favède, C. Predella, O. Reynard, S. Durand, M. Mazelier, E. Pizzioli, D. Decimo, F.T. Bovier, L.M. Lapsley, C. Castagna, N.A.P. Lieberman, G. Noel, C. Mathieu, B. Malissen, T. Briese, A.L. Greninger, C.A. Alabi, N.V. Dorrello, S. Marot, A.-G. Marcelin, A. Zarubica, A. Moscona, M. Porotto, B. Horvat, Intranasally administrated fusion-inhibitory lipopeptides block SARS-CoV-2 infection in mice and enable long-term protective immunity, Commun. Biol. 8 (1) (2025) 57, https://doi.org/10.1038/s42003-025-07491-4.

[20] Y. Hu, Y. Zhu, Y. Yu, N. Liu, X. Ju, Q. Ding, Y. He, Design and characterization of novel SARS-CoV-2 fusion inhibitors with N-Terminally extended HR2 peptides, Antivir. Res. 212 (2023) 105571, https://doi.org/10.1016/j.antiviral.2023.105571.

[21] C. Wang, Q. Li, Y. Wang, W. Zhang, L. Zheng, J. Tu, J. Zhou, F. Wang, Y. Yuan, B. Xu, G. Xue, X. Du, M. Yuan, S. Du, H. Wang, X. Zhuang, W. Shi, L. Lu, J. Xiao, Q. Wang, S. Jiang, Potent inhibition of human betacoronaviruses by a short double-stapled peptide mimicking the HR2 core region in viral spike protein, J. Med. Chem. 68 (17) (2025) 18625–18640, https://doi.org/10.1021/acs.jmedchem.5c01614.

[22] Y. Liao, S.M. Zhang, T.L. Neo, J.P. Tam, Tryptophan-dependent membrane interaction and heteromerization with the internal fusion peptide by the membrane proximal external region of SARS-CoV spike protein, Biochemistry 54 (9) (2015) 1819–1830, https://doi.org/10.1021/bi501352u.

[23] S. Giannecchini, F. Bonci, M. Pistello, D. Matteucci, O. Sichi, P. Rovero, M. Bendinelli, The membrane-proximal tryptophan-rich region in the transmembrane glycoprotein ectodomain of feline immunodeficiency virus is important for cell entry, Virology 320 (1) (2004) 156–166, https://doi.org/10.1016/j.virol.2003.12.001.

[24] S. Giannecchini, A. Di Fenza, A.M. D'Ursi, D. Matteucci, P. Rovero, M. Bendinelli, Antiviral activity and conformational features of an octapeptide derived from the membrane-proximal ectodomain of the feline immunodeficiency virus transmembrane glycoprotein, J. Virol. 77 (6) (2003) 3724–3733, https://doi.org/10.1128/jvi.77.6.3724-3733.2003.

[25] L.K. Regula, R. Harris, F. Wang, C.D. Higgins, J.F. Koellhoffer, Y. Zhao, K. Chandran, J. Gao, M.E. Girvin, J.R. Lai, Conformational properties of peptides corresponding to the Ebolavirus GP2 membrane-proximal external region in the presence of micelle-forming surfactants and lipids, Biochemistry 52 (20) (2013) 3393–3404, https://doi.org/10.1021/bi400040v.

[26] V. Buzon, G. Natrajan, D. Schibli, F. Campelo, M.M. Kozlov, W. Weissenhorn, Crystal structure of HIV-1 Gp41 including both fusion peptide and membrane proximal external regions, PLoS Pathog. 6 (5) (2010) e1000880, https://doi.org/10.1371/journal.ppat.1000880.

[27] A.K. Bellamy-McIntyre, C.-S. Lay, S. Baaör, A.L. Maerz, G.H. Talbo, H.E. Drummer, P. Poumbourios, Functional links between the fusion peptide-proximal polar segment and membrane-proximal region of human immunodeficiency virus Gp41 in distinct phases of membrane fusion, J. Biol. Chem. 282 (32) (2007) 23104–23116, https://doi.org/10.1074/jbc.M703485200.

[28] G. Freer, S. Giannecchini, A. Tissot, M.F. Bachmann, P. Rovero, P.F. Serres, M. Bendinelli, Dissection of seroreactivity against the tryptophan-rich motif of the feline immunodeficiency virus transmembrane glycoprotein, Virology 322 (2) (2004) 360–369, https://doi.org/10.1016/j.virol.2004.02.017.

[29] J. Huang, G. Ofek, L. Laub, M.K. Louder, N.A. Doria-Rose, N.S. Longo, H. Imamichi, R.T. Bailer, B. Chakrabarti, S.K. Sharma, S.M. Alam, T. Wang, Y. Yang, B. Zhang, S. A. Migueles, R. Wyatt, B.F. Haynes, P.D. Kwong, J.R. Mascola, M. Connors, Broad and potent neutralization of HIV-1 by a Gp41-Specific human antibody, Nature 491 (7424) (2012) 406–412, https://doi.org/10.1038/nature11544.

[30] M.A. Stincarelli, M. Quagliata, A. Di Santo, L. Pacini, F.R. Fernandez, R. Arvia, S. Rinaldi, A.M. Papini, P. Rovero, S. Giannecchini, SARS-CoV-2 inhibitory activity of a short peptide derived from internal fusion peptide of S2 subunit of spike glycoprotein, Virus Res. 334 (2023) 199170, https://doi.org/10.1016/j.virusres.2023.199170.

[31] M. Ferrer, T.M. Kapoor, T. Strassmaier, W. Weissenhorn, J.J. Skehel, D. Oprian, S. L. Schreiber, D.C. Wiley, S.C. Harrison, Selection of Gp41-Mediated HIV-1 cell entry inhibitors from biased combinatorial libraries of non-natural binding elements, Nat. Struct. Biol. 6 (10) (1999) 953–960, https://doi.org/10.1038/13324.

[32] P. Khandelwal, S. Seth, V. Hosur, R. CD and NMR investigations on trifluoroethanol-induced step-wise folding of helical segment from scorpion neurotoxin, Eur. J. Biochem. 264 (2) (1999) 468–478, https://doi.org/10.1046/j.1432-1327.1999.00641.x.

[33] M. Buck, Trifluoroethanol and colleagues: cosolvents come of age. Recent studies with peptides and proteins, Q. Rev. Biophys. 31 (3) (1998) 297–355, https://doi.org/10.1017/S003358359800345X.

[34] D. Wang, K. Chen, J.L. Kulp Iii, P.S. Arora, Evaluation of biologically relevant short alpha-helices stabilized by a main-chain hydrogen-bond surrogate, J. Am. Chem. Soc. 128 (28) (2006) 9248–9256, https://doi.org/10.1021/ja062710w.

[35] L. Zhang, J. Hermans, 310 Helix versus .Alpha.-Helix: a molecular dynamics study of conformational preferences of aib and alanine, J. Am. Chem. Soc. 116 (26) (1994) 11915–11921, https://doi.org/10.1021/ja00105a034.

[36] A.S. Ladokhin, M.E. Selsted, S.H. White, CD spectra of indolicidin antimicrobial peptides suggest turns, not polyproline Helix, Biochemistry 38 (38) (1999) 12313–12319, https://doi.org/10.1021/bi9907936.

[37] C.R. Martinez, B.L. Iverson, Rethinking the term "Pi-Stacking.", Chem. Sci. 3 (7) (2012) 2191–2201, https://doi.org/10.1039/C2SC20045G.

[38] M.-A. Sani, S. Rajput, D.W. Keizer, F. Separovic, NMR techniques for investigating antimicrobial peptides in model membranes and bacterial cells, Methods 224 (2024) 10–20, https://doi.org/10.1016/j.ymeth.2024.01.012.

[39] D.A. Kallick, M.R. Tessmer, C.R. Watts, C.Y. Li, The use of dodecylphosphocholine micelles in solution NMR, J. Magn. Reson. B 109 (1) (1995) 60–65, https://doi.org/10.1006/jmrb.1995.1146.

[40] W. Shi, Y. Cai, H. Zhu, H. Peng, J. Voyer, S. Rits-Volloch, H. Cao, M.L. Mayer, K. Song, C. Xu, J. Lu, J. Zhang, B. Chen, Cryo-EM structure of SARS-CoV-2 postfusion spike in membrane, Nature 619 (7969) (2023) 403–409, https://doi.org/10.1038/s41586-023-06273-4.

[41] A. Elalouf, H. Elalouf, H. Maoz, A. Elalouf, H. Elalouf, H. Maoz, HIV-1 entry mechanisms: protein-host receptor interactions and membrane fusion dynamics, Front. Biosci.-Landmark 30 (10) (2025), https://doi.org/10.31083/FBL37412.

[42] D.J. Schibli, W. Weissenhorn, Class I and class II viral fusion protein structures reveal similar principles in membrane fusion (Review), Mol. Membr. Biol. 21 (6) (2004) 361–371, https://doi.org/10.1080/09687860400017784.
[43] M. Quagliata, P. Rovero, M. Chorev, A.M. Papini, Advances in the synthesis of cyclic peptides, pseudopeptides, and peptoids by CuAAC-Mediated macrocyclization, Trends Chem. 7 (6) (2025) 276–298, https://doi.org/10.1016/j.trechm.2025.04.004.
[44] S.P. Skinner, R.H. Fogh, W. Boucher, T.J. Ragan, L.G. Mureddu, G.W. Vuister, CcpNmr Analysis Assign: a flexible platform for integrated NMR analysis, J. Biomol. NMR 66 (2) (2016) 111–124, https://doi.org/10.1007/s10858-016-0060-y.
[45] P. Klukowski, F.F. Damberger, F.H.-T. Allain, H. Iwai, H. Kadavath, T.A. Ramelot, G.T. Montelione, R. Riek, P. Güntert, The 100-Protein NMR spectra dataset: a resource for biomolecular NMR data analysis, Sci. Data 11 (2024) 30, https://doi.org/10.1038/s41597-023-02879-5.
[46] Y. Kim, G. Jang, D. Lee, N. Kim, J.W. Seon, Y.-H. Kim, C. Lee, Trypsin enhances SARS-CoV-2 infection by facilitating viral entry, Arch. Virol. 167 (2) (2022) 441–458, https://doi.org/10.1007/s00705-021-05343-0.